


Modified input-to-output and control-to-output transfer functions of a non-ideal buck converter working in discontinuous conduction mode

MARCIN WALCZAK  

*Department of Electronics and Computer Science, Koszalin University of Technology,
Śniadeckich 2 str., 75-453 Koszalin, Poland
e-mail:  marcin.walczak@tu.koszalin.pl*

(Received: 10.03.2024, revised: 22.11.2024)

Abstract: Small-signal models of a buck converter working in the discontinuous conduction mode that are available in the literature usually can be divided into those which contain a single pole and refer to non-ideal converters and those that describe ideal converters and contain two poles. Even though the models are noticeably different they have been validated through simulations and measurements, which suggests both of them are correct. The purpose of this paper is to provide a comprehensive comparison of the existing models with transient simulations done in OrCAD software and through measurements, to show that both of the mentioned models are true for a specific set of converter parameters, and to propose a two-pole, control-to-output and input-to-output transfer functions of a non-ideal buck converter, that can be used in any buck converter working in discontinuous conduction mode.

Key words: buck converter, control-to-output, input-to-output, small-signal model, transfer function

1. Introduction

Small-signal models are fundamental in analysis of the dc-dc converters. The models describe the behaviour of a specific converter based on its type (topology) and the mode of operation. They provide information on converters' dynamics and are essential for designing the classic control system [1], that ensures the output voltage meets specific requirements. Over the years a few of the modelling methods have been proposed. Every time a new method was introduced it was to try a different modelling approach or to simplify the modelling process. However, the newest articles show that there are still areas within the modelling of DC/DC converters that can be addressed and improved [2, 3]. One of the most popular modelling techniques is the state-space averaging



© 2024. The Author(s). This is an open-access article distributed under the terms of the Creative Commons Attribution-NonCommercial-NoDerivatives License (CC BY-NC-ND 4.0, <https://creativecommons.org/licenses/by-nc-nd/4.0/>), which permits use, distribution, and reproduction in any medium, provided that the Article is properly cited, the use is non-commercial, and no modifications or adaptations are made.

introduced in 1976 [4]. It was initially used to describe ideal converters working in the continuous conduction mode (CCM). However, in the article it was mentioned that this technique can also be used for converters working in the discontinuous conduction mode (DCM). The converters working in DCM feature substantially different frequency responses than converters in CCM, therefore they require an alternative modelling approach. However, in [5] it was noted that utilizing the SSA technique in for DCM can produce inaccurate models if no modifications are done to the SSA matrices. Moreover, the authors stated that models of buck and boost converters working in DCM should include a second pole, which is located at high frequencies. Since then the resulting models have been divided into reduced order models (including a single-pole transfer function), full order models (that contain two poles) and corrected full order models (which include two poles and take into consideration the proposed modification of the SSA matrices) [6, 7].

Another popular modelling technique is PWM switch averaging [8, 9]. However, there is also an energy-conservation approach [10] and separation of the variable method [11]. All of the techniques utilise the same steps, namely averaging, perturbation and linearization, and thus if correctly applied lead to the same results – i.e. models that are an approximation of the actual signals. As such their accuracy is limited. Usually, the models are assumed to be valid within 1/3 of the switching frequency [5, 7]. However even within the frequency window, the accuracy of the models depends on their complexity. To increase the accuracy, various parasitic effects, such as equivalent series resistances (ESRs), have to be taken into account. Therefore, the full order models were derived including different parasitic resistances [12–16] and some of them utilized a different diode model [17, 18]. The models that include all of the resistances can be found in the literature [13, 17, 19]. However, in most cases, the models describe the behaviour of the converters working in the continuous conduction mode. As it turns out, deriving small-signal models with the parasitic resistances for the converters working in the DCM is much more complicated than doing it for CCM – even for the basic buck or boost converters. Working with discontinuous conduction mode has some disadvantages. The converters operating in DCM have higher current ripple than those operating in continuous conduction mode. This leads to higher stress on the components of the converter. However, DCM is still preferred for low-power applications since it is more cost-effective and smaller in size compared to converters operating in CCM [20]. Some of the existing papers contain results of the simulations that include the parasitic resistances [21–23], however the presented formulas can be divided into two categories – papers that include single pole transfer functions, and those that use two-pole models, however the models are presented only as the initial formula and not the transfer function [7]. Nevertheless, both of the ideas (a single-pole and two-pole models) are backed up with simulations and measurements that prove their validity, even though in most cases they produce different results.

The purpose of this paper is to present and verify two-pole small-signal models of a buck converter, that include the parasitic resistances of all of the converter components. Moreover, this paper shows that the available single-pole and two-pole small-signal models are correct for specific conditions (i.e. a specific set of converter parameters), and thus cannot predict the behaviour of the converters if the conditions are not met, unlike the presented model. One of the models, namely the control-to-output transfer function of a non-ideal buck converter working in the discontinuous conduction mode, has already been presented in the PhD thesis [24]. However, because of the language barrier, its range is limited, therefore it is being evaluated in this paper. The second model input-to-output transfer function has never been published before.

Section 2 describes how the presented models were derived using the separation of variable method. Section 3 includes information on the simulation and measurement setup details. It describes methods that have been utilised to acquire the presented frequency characteristics. The comparison of the proposed model with the simulation and the measurement can be found in Section 4. The section also includes the discussion of the results, which are followed by conclusions in Section 5.

2. Derivation of the small-signal models

A single pole control-to-output transfer function of a buck converter working in the discontinuous conduction mode (DCM) can be derived through the assumption that the average voltage across the inductor (over one switching cycle) is equal to zero [11]. If an ideal converter is the subject to the derivation a single-pole small-signal model is achieved [25], sec.11.3. The model features only a single pole and no zeros. This model is easy to derive but is not very useful for practical implementation due to its accuracy. For better accuracy, the parasitic resistances of the converter's components have to be taken into account, which results in an additional zero in the small-signal model. The location of the zero depends on the equivalent series resistance (ESR) of the output capacitor [11]. This model has been proven to be correct, however according to [5, 25] a buck converter working in the DCM features a second pole, which also has been proven to be true in [5]. However, the models presented there refer to ideal converters only. In [7] a two-pole model with zero corresponding to the parasitic resistance of the output capacitor has been analysed and confirmed, but the paper did not present the model in the form of a transfer function. To derive the two-pole transfer function, which would include the parasitic resistances corresponding to all components of the converter, the assumption stating that the average value of the inductor voltage over a switching cycle is equal to zero, has to be changed. This will allow us to take the path that will lead to a two-pole model.

In discontinuous conduction mode, one period of the switching signal can be divided into three intervals (Fig. 1). The first interval corresponds to the ON phase of the transistor switch and is directly related to the duty cycle d_A . During this interval, the inductor current rises until the switching signal changes its state to a low level at t_1 .

After the transistor switch is turned off, the inductor current starts to drop. The time between t_1 and the point when the inductor current reaches zero value at t_2 can be described as $d_1 T_S$. The rest of the period between t_2 and T_S , where the inductor current is zero, can be described as $(1 - d_A - d_1) T_S$. Since the t_1 is known because of its direct relation to the PWM signal, only the value d_1 has to be found and described using the parameters of the converter. Before doing that, it is important to distinguish two values, namely an inductor current averaged over a specific interval $i_{LAV(ON)}$ and the inductor current averaged over the whole period i_{LAV} – the visual explanation is presented in Fig. 1. When those two values are established the modelling can start. For the modelling process of a non-ideal buck converter, a circuit shown in Fig. 2 will be used. The circuit includes parasitic resistances of the converter components. The complete list of the symbols used in this section can be found in the Appendix (Table A1).

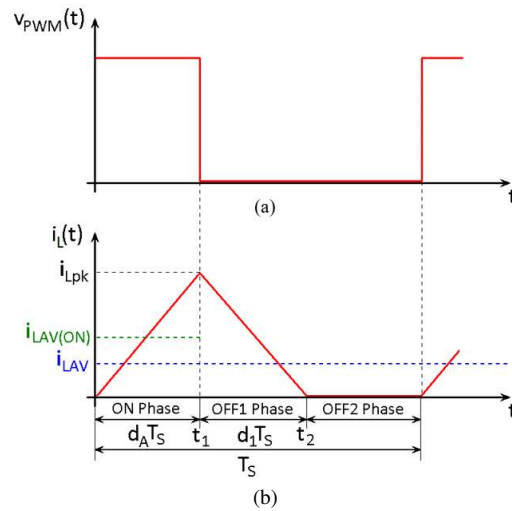


Fig. 1. Current phases and current averaged values in discontinuous conduction mode: (a) PWM signal; (b) inductor current

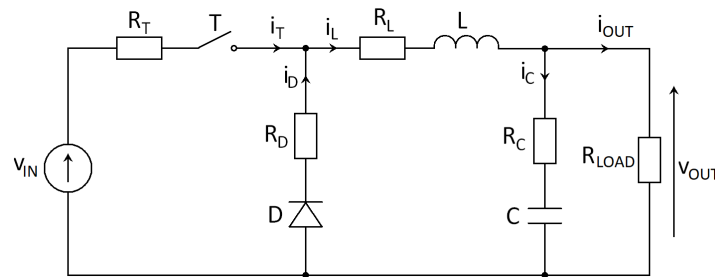


Fig. 2. A nonideal buck converter

At first, all equations related to Kirchhoff's laws can be written down. Thus, the voltage and current equations can be written as (1)–(3).

$$v_{LAV} = (v_{IN} - i_{LAV(ON)}(R_L + R_T) - v_{OUT}) d_A + (-i_{LAV(OFF1)}(R_L + R_D) - v_{OUT}) d_1, \quad (1)$$

$$v_{OUT} - v_C - i_C R_C = 0, \quad (2)$$

$$i_L - i_C - i_{OUT} = 0. \quad (3)$$

There are some unknown values in (1)–(3) that have to be represented by known values, and so d_1 can be calculated using the peak value of the inductor current i_{Lpk} , and the average value of the inductor current calculated over the whole period i_{LAV} . The peak value of the inductor current i_{Lpk} is an integral of the inductor voltage over time, divided by the inductance, and thus, after including the parasitic resistances, it can be described as (4).

$$i_{Lpk} = \frac{v_{IN} - i_{LAV(ON)}(R_T + R_L) - v_{OUT}}{L} d_A T_S. \quad (4)$$

The average value of the inductor current calculated over the whole period T_S is represented by (5)

$$i_{LAV} = \frac{i_{Lpk}}{2}(d_A + d_1). \quad (5)$$

The formula for d_1 can be calculated as a product of (4) and (5). By substituting (4) into (5) and solving the equation for d_1 one gets (6),

$$d_1 = \frac{R_G i_{LAV}}{(v_{IN} - v_{OUT} - i_{LAV(ON)} R_P) d_A} - d_A. \quad (6)$$

For simplification some of the values have been replaced by the following coefficients:

$$R_G = \frac{2L}{T_S}, \quad (7)$$

$$R_P = R_T + R_L. \quad (8)$$

The averaged inductor current calculated in the ON phase $i_{LAV(ON)}$ is equal to the half of the inductor current peak value i_{Lpk} , therefore by updating (4) using (7)–(8) we get:

$$i_{LAV(ON)} = \frac{i_{Lpk}}{2} = \frac{v_{IN} - i_{LAV(ON)} R_P - v_{OUT}}{R_G} d_A. \quad (9)$$

Solving (9) for $i_{LAV(ON)}$ gives the final value for the inductor current averaged over the ON phase

$$i_{LAV(ON)} = \frac{v_{IN} - v_{OUT}}{R_G + R_P d_A} d_A. \quad (10)$$

Introducing (6)–(8) into (1) and stating that the average values of the inductor current in the ON and OFF1 phase are the same $i_{LAV(ON)} = i_{LAV(OFF1)}$, it is possible to calculate the formula for the inductor voltage, that has been averaged over the whole period v_{LAV} (11).

$$v_{LAV} = \frac{R_G (-i_{LAV(ON)} R_P - v_{OUT})}{(v_{IN} - v_{OUT} - i_{LAV(ON)} R_P) d_A} i_{LAV}. \quad (11)$$

Equation (11) is the first equation required for calculating the transfer functions. Equations (2) and (3) can be used to derive the second formula. For this the output capacitor current i_C in (2) and (3) has to be substituted by a formula for the capacitor current (12). Next, the operation of perturbation has to be performed on both of the equations. After linearization and calculating the Laplace transformation, it is possible to solve one of the equations for v_C (13). Subsequently, the formula needs to be introduced to the Laplace transformation of (3), thus removing the value of capacitor voltage v_C out of the equation. As a result, we get (14).

$$i_C = C \frac{dv_C}{dt}, \quad (12)$$

$$V_C(s) = \frac{V_{out}(s)}{1 + sCR_C}, \quad (13)$$

$$V_C(s) = \frac{V_{out}(s)}{1 + sCR_C}. \quad (14)$$

Equation (14) is the second equation required for calculating the transfer functions. To move forward (11) and (14) have to be presented in the form of (15) and (16). It can be noticed that (14) already looks like (16) therefore the coefficients $\beta_1 - \beta_4$ can be easily determined. However, to get the coefficients $\alpha_1 - \alpha_4$ in (15) it is required to calculate partial derivatives from (11) according to (17)–(20).

$$sLI_L(s) = \alpha_1 I_L(s) + \alpha_2 \theta(s) + \alpha_3 V_{\text{out}}(s) + \alpha_4 V_{\text{in}}(s), \quad (15)$$

$$sCV_{\text{out}}(s) = \beta_1 I_L(s) + \beta_2 \theta(s) + \beta_3 V_{\text{out}}(s) + \beta_4 V_{\text{in}}(s), \quad (16)$$

where:

$$\alpha_1 = \frac{dv_L}{di_L}, \quad (17)$$

$$\alpha_2 = \frac{dv_L}{d\theta}, \quad (18)$$

$$\alpha_3 = \frac{dv_L}{dv_{\text{OUT}}}, \quad (19)$$

$$\alpha_4 = \frac{dv_L}{dv_{\text{IN}}}. \quad (20)$$

When the coefficients are known, the formulas for transfer functions can be calculated directly from (15) and (16):

$$H_d(s) = \left. \frac{V_{\text{out}}(s)}{\theta(s)} \right|_{V_{\text{in}}(s)=0} = \frac{\beta_1 \alpha_2 + \beta_2 (sL - \alpha_1)}{(sC - \beta_3)(sL - \alpha_1) - \beta_1 \alpha_3}, \quad (21)$$

$$H_g(s) = \left. \frac{V_{\text{out}}(s)}{V_{\text{in}}(s)} \right|_{\theta(s)=0} = \frac{\beta_1 \alpha_4 + \beta_4 (sL - \alpha_1)}{(sC - \beta_3)(sL - \alpha_1) - \beta_1 \alpha_3}. \quad (22)$$

The final version of (21) and (22) are given as (23) and (24), respectively. The formulas for the coefficients can be found in the Appendix (A.1–A.11).

$$H_d(s) = \frac{K(KV_{\text{IN}}D_A^2 + R_G V_{\text{OUT}}G)(sCRc + 1)}{C_Z L K^2 D_A^2 s^2 + (GLK^2 D_A^2 + C_Z M_I R_\gamma K D_A^2 + CGM_I R_C R_{PG} D_A)s + GM_I D_A (R_{PG} + R_\gamma K D_A)}, \quad (23)$$

$$H_g(s) = \frac{(K^2 D_A^2 + R_{PG}G)(sCRc + 1)D_A}{C_Z L K^2 D_A^2 s^2 + (GLK^2 D_A^2 + C_Z M_I R_\gamma K D_A^2 + CGM_I R_C R_{PG} D_A)s + GM_I D_A (R_{PG} + R_\gamma K D_A)}. \quad (24)$$

3. Materials and methods

3.1. DC–DC converter

To evaluate the small-signal models of a nonideal buck converter a transient simulation using OrCAD has been performed. A general schematic of the converters is presented in Fig. 2. To provide comprehensive results three converters with different component values were chosen for the simulation. The component values were carefully selected for each converter so that all of the chosen small-signal models could be evaluated. Thus, in the first converter, the inductor and the output capacitor values were chosen to set the two poles relatively close to each other – the low-frequency pole was set above 1/100 and below 1/10 of the switching frequency, whereas the

high-frequency pole was set in the frequency range between 100 kHz and 300 kHz. This way the second pole will still affect the measurements, which according to the literature can be done up to 1/3 of the switching frequency. It can be noticed that the output capacitance of the first converter is relatively small however, small capacitances on the output of the converter can be found in the literature [7, 26] and are not uncommon, especially when the switching frequency and the inductor values are relatively high. Nevertheless, such value of the output capacitance has been chosen on purpose to show differences between the small-signal models. In the first converter, the potential zero related to the small-signal model is far beyond the switching frequency, therefore its influence on the frequency characteristics is negligible.

The second converter contains elements that set the first pole at lower frequencies – i.e. below 50 Hz so that the influence of the zero and the second pole could be observed on the frequency characteristics. As for the zero and second pole they have been set in the vicinity of the switching frequency, however, the zero is placed below the switching frequency and the second pole was set above it. This way the phase characteristic should curve upward for frequencies larger than 10 kHz.

In the third converter, the first pole is set at low frequencies (below 50 Hz) and the second pole is moved to high frequencies so that its influence on the frequency characteristics is reduced. The zero of the small-signal model was set below 1/10 of the switching frequency f_S . Table 1 contains all of the component values used in the simulations and measurements. The values were determined based on the measurements of physical components. The equivalent series resistances of the capacitors and inductors were measured using an RLC bridge FLUKE PM6306, whereas the values of the transistor and diode resistances were evaluated based on the measurements of the static characteristics.

Table 1. The values of the components used in the simulation

Name	Symbol	buck_1	buck_2	buck_3
Inductance	L [μH]	95.8	90.8	32
Capacitance of the output capacitor	C [μF]	1.1	108.8	330
Load resistance	R_{LOAD} [Ω]	198	198	198
Diode	–	MBRS340	MBRS340	MBRS340
Transistor	–	NVD5867NLT4G	NVD5867NLT4G	AP9962GH
ESR of the inductor	R_L [$\text{m}\Omega$]	133.8	121	53
ESR of the capacitor	R_C [$\text{m}\Omega$]	121	18.6	96 ^[a]
$R_{\text{DS(ON)}}$ resistance of the transistor	R_T [$\text{m}\Omega$]	39	39	20
Diode resistance	R_D [$\text{m}\Omega$]	281	281	281
Input voltage of the converter	V_{IN} [V]	8	8	8
Switching frequency of the PWM signal	f_S [Hz]	100 000	100 000	100 000
CCM/DCM boundary resistance ^[b]	R_{crit} [Ω]	47.9	45.4	16

[a] Resistance of an electrolytic capacitor

[b] The smallest value of the load resistance that puts the converter into the DCM mode, calculated according to [27]

The small-signal models of a non-ideal buck converter working in DCM, which are presented in this paper, were derived using a method presented in [5] and [21]. One of the models (control-to-output) describes the relation between the averaged values of the converter's output voltage and the duty cycle d_A of the PWM signal that drives the high-side transistor. The second model (input-to-output) describes the relation between the averaged values of the converter's output and input voltages. In contrast to other models that can be found in the literature, the presented ones feature two poles and include the parasitic resistances of the converter components. Moreover, the proposed models are presented in the form of a transfer function, which can be used for quick analysis, simulations and design of the control system.

As mentioned before, the presented models are two-pole transfer functions that include parasitic resistances of the elements used in a buck converter. The advantages of the two-pole models have already been presented in the literature. However, the models that include only one pole are still valid in some cases. To show all of the advantages and disadvantages of the models, three other transfer functions have been chosen for the comparison – namely:

- single-pole model of an ideal converter [25], sec. 11.2,
- single-pole model of a non-ideal converter [21], sec. 5.3.7,
- two-pole model of an ideal converter [25], sec. 11.3.

3.2. Simulation

The most common way to test a small-signal model is to compare it to a simulation or a measurement done in the frequency domain. Since the presented models are control-to-output and input-to-output transfer functions, therefore two test circuits have to be used. The circuit shown in Fig. 3 was used to simulate the control-to-output frequency characteristics. In this circuit, the PWM control signal is generated as a combination of two voltage sources – a sinusoidal v_{SIN} and a sawtooth v_{SAW} . The offset and amplitude of the sinusoidal signal determine the quiescent value D_A and perturbation amplitude $d_a(t)$ of the PWM duty cycle respectively, as shown in Fig. 4. Subsequently, the modulated PWM signal is fed to the switching element and thus influences the output signal. The frequency of the v_{SAW} determines the frequency of the PWM signal therefore it is constant. Whereas the frequency of v_{SIN} determines the perturbation frequency of the PWM signal therefore it is changed for every point at the frequency characteristic.

Figure 5 was used to simulate the input-to-output frequency characteristics. The sinusoidal component of the input voltage v_{IN} provides perturbation of the input voltage. The duty cycle is constant throughout the whole simulation.

An ideal switch S1 shown in Figs. 3 and 5 was used to simulate the switching properties of a transistor. The on and off resistances of the switch were set to $1 \mu\Omega$ and $1 M\Omega$, respectively. An additional resistance R_t was added in series to the switch to simulate the ON resistance of the transistor.

The simulations were done using OrCAD software that calculated the output signal v_{OUT} in the time domain for various frequencies of the sinusoidal voltage source v_{SIN} .

An example of v_{SIN} and v_{OUT} signals calculated in input-to-output simulation for a single frequency is shown in Fig. 6. The mean values of the signals were removed to show the AC component.

It can be noticed that the output signal in Fig. 6 contains high-frequency harmonics. Those harmonics correspond to the PWM signal and they exist in every converter. The amplitude of the harmonics depends on the parameters of the converter. During the gain and phase shift

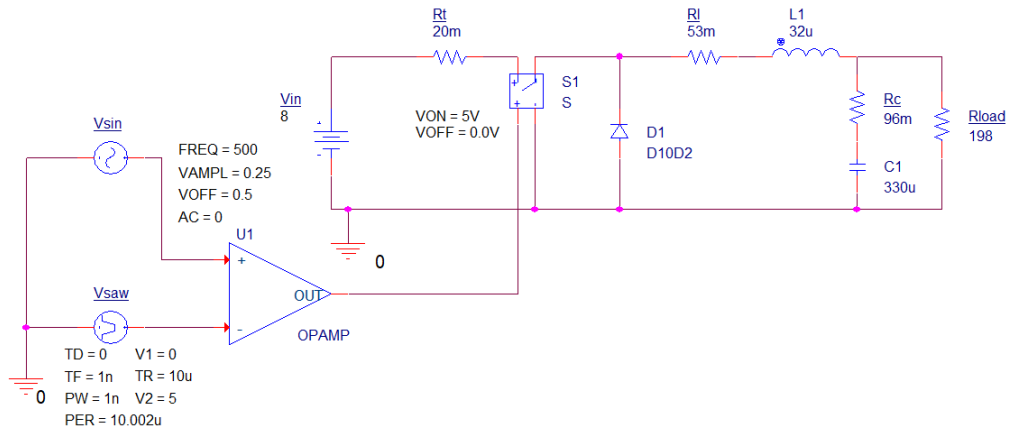


Fig. 3. Circuit used for simulation of control-to-output frequency characteristic of the buck converters working in discontinuous conduction mode

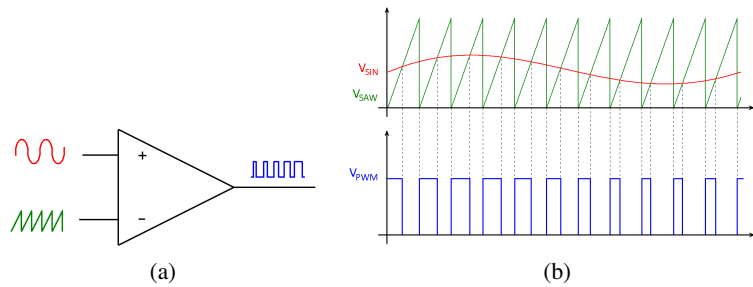


Fig. 4. The principle of PWM signal generation for the control-to-output simulation: (a) connection; (b) signals

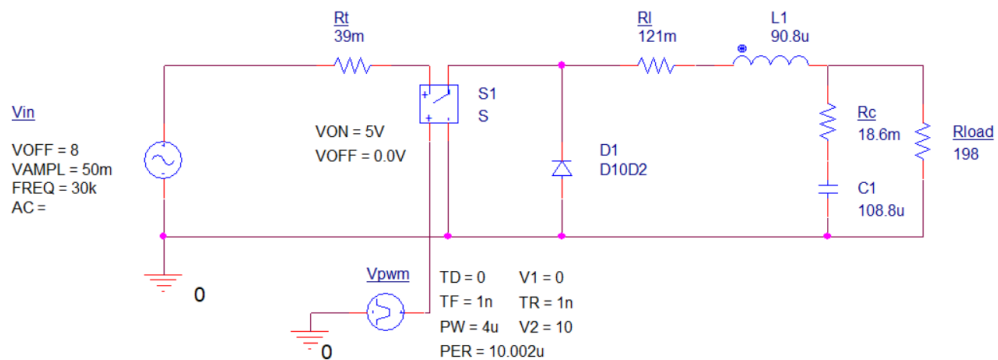


Fig. 5. Circuit used for simulation of input-to-output frequency characteristic of the buck converters working in discontinuous conduction mode

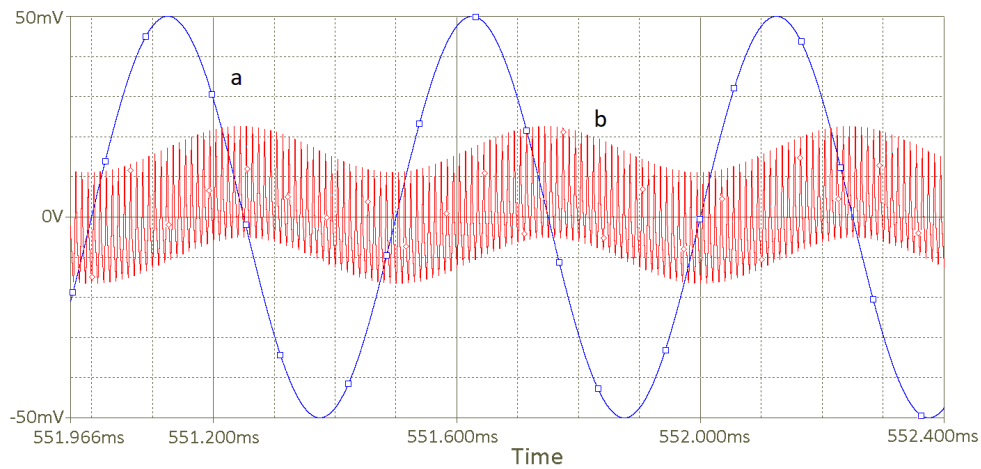


Fig. 6. Result of input-to-output simulation showing: (a) input signal (v_{IN}); (b) output voltage

measurements, especially if they are done at higher frequencies, those harmonics become more noticeable due to the decreasing amplitude of the output signal. This makes the measurement quite difficult and requires using an indirect approach. To draw the frequency characteristics presented in this paper, the input and output signals, related to a specific frequency, were analysed and compared using the FFT method presented in [28]. The method uses FFT to extract information about the amplitude and phase shift from the signals in the time domain. However, due to the irregular point distribution in the waveforms produced by OrCAD software, the results of the simulations had to be processed first, before feeding them to the FFT algorithm. The purpose of the processing was to remove redundant points from the simulation and leave only data with a constant sampling ratio (Fig. 7).

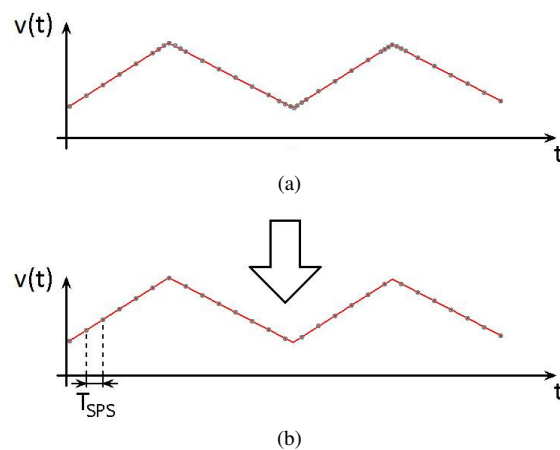


Fig. 7. The idea of removing the redundant samples from OrCAD simulation: (a) simulation result; (b) signal with reduced number of samples

To provide good accuracy the maximum step size during the simulation was set to 10 ns. The data were gathered between 500 ms and 600 ms to ensure that the converter works in the steady-state region. After the removal of the redundant points, the resulting data featured a constant sampling frequency of 20 MSPS which enabled further processing.

3.3. Measurements

Measurements of the frequency characteristics were done using the same principle as for the simulation i.e. by measuring the input and output signals in the time domain and using the FFT to extract information on the amplitude and phase shift for specific frequencies. The measurement setup featuring Tektronix AFG3022B generator, Tektronix MSO5104 oscilloscope, LPS-305 and LPS-304 bench power supplies and load resistors mounted on a radiator, is presented in Fig. 8.

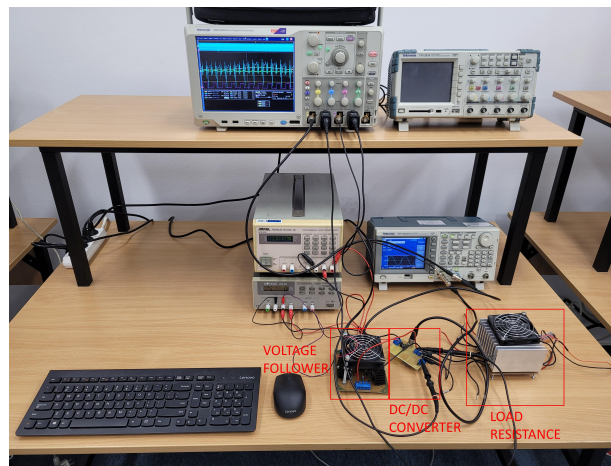


Fig. 8. The measurement setup

For the measurements of the H_d transfer function, a TL3016 comparator was used to generate the modulated PWM signal. The comparator features a 7.6 ns delay, which is small enough to not affect the phase shift noticeably (at least within the measured frequency range). The circuit of the PWM modulator is presented in Fig. 9. The sawtooth signal was connected to the positive input of the comparator, which means that when the DC component of the sinusoidal voltage increased the steady-state value of the duty cycle decreased. Therefore, to get the right value of the phase shift the input signal had to be shifted by 180 degrees. Additionally, to minimize the influence of current oscillations, that appear in DCM, on the frequency characteristics an RC snubber was used in parallel with the diode.

Measurements of the H_g transfer function required an additional circuit to provide a DC voltage with an AC component. The AFG3022B generator did not provide enough current therefore a voltage follower built with three OPA549 operational amplifiers with proper cooling was used. The circuit featured 98 kHz bandwidth and over 3 A of a continuous current, which was sufficient for the measurements of the H_g transfer function. The voltages were measured directly at the input and output of the converter. The circuit of the voltage follower is presented in Fig. 10.

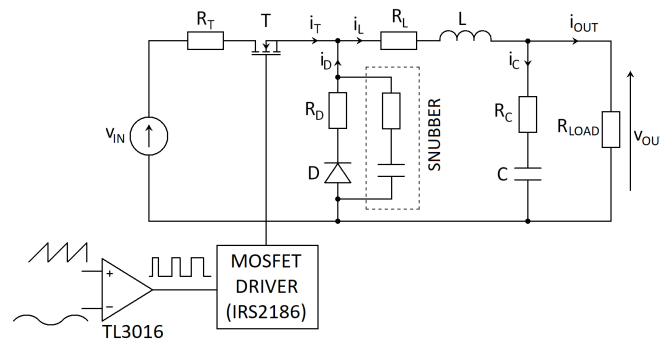


Fig. 9. The circuit used for frequency characteristic measurements of the control-to-output transfer function

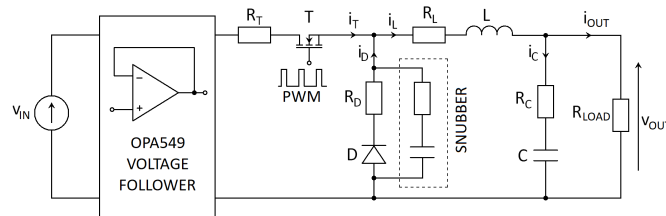


Fig. 10. The circuit used for frequency characteristic measurements of the input-to-output transfer function

4. Results

4.1. Simulation and measurement results

The results of the calculations, simulations and the measurements of the control-to-output transfer functions for the duty cycles of 0.1 and 0.4 are presented in Figs. 11–13 and Figs. 14–16, respectively. The curves marked as 1 corresponds to the single-pole model of an ideal buck converter. Curves marked as 2 represent the single-pole model of a non-ideal converter. Curves 3 refer to the two-pole model of an ideal buck converter. Whereas the curves 4 is the representation of the proposed two-pole model of a non-ideal buck converter. The black circles on the figures represent values acquired throughout the simulation done in OrCAD. The measurement results are shown as the red dots.

The results of the calculations, simulations and the measurements of the input-to-output transfer functions for the duty cycles of 0.1 and 0.4 are presented in Figs. 17–19 and Figs. 20–22, respectively. The curves marked as 1 corresponds to the single-pole model of an ideal buck converter. Curves marked as 2 represent the single-pole model of a non-ideal converter. Curves 3 refer to the two-pole model of an ideal buck converter. Whereas curves 4 are the representation of the proposed two-pole model of a non-ideal buck converter. The black circles on the figures represent values acquired throughout the simulation done in OrCAD. The measurement results are shown as the red dots.

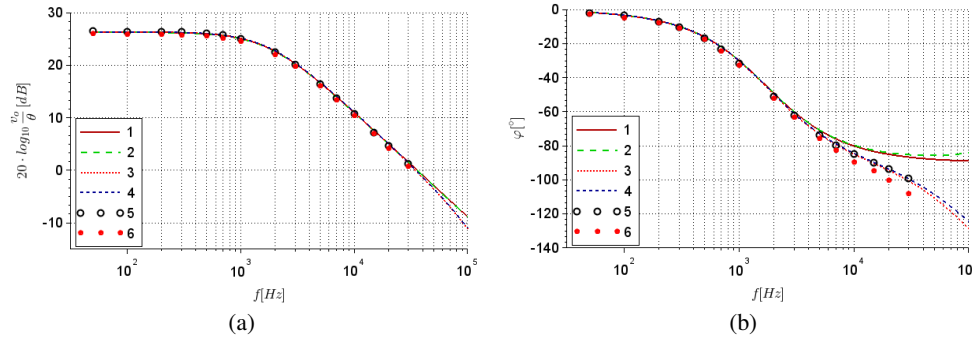


Fig. 11. Control-to-output (H_d) frequency characteristics of the buck_1 converter (buck_1), working in DCM with duty cycle $D_A = 0.1$. The curves correspond to: 1 – single-pole model of an ideal converter; 2 – single-pole model of a non-ideal converter; 3 – two-pole model of an ideal converter; 4 – proposed two-pole model of a non-ideal converter; \circ – simulation results; \bullet – measurement results

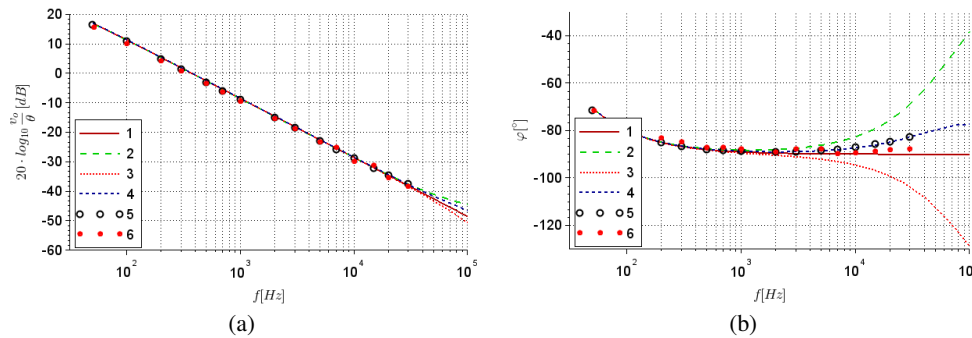


Fig. 12. Control-to-output (H_d) frequency characteristics of the buck_2 converter working in DCM with duty cycle $D_A = 0.1$. The curves correspond to: 1 – single-pole model of an ideal converter; 2 – single-pole model of a non-ideal converter; 3 – two-pole model of an ideal converter; 4 – proposed two-pole model of a non-ideal converter; \circ – simulation results; \bullet – measurement results

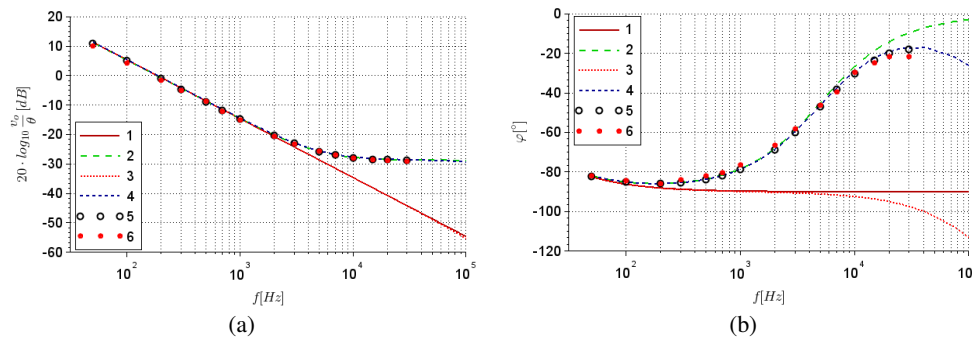


Fig. 13. Control-to-output (H_d) frequency characteristics of the buck_3 converter working in DCM with duty cycle $D_A = 0.1$. The curves correspond to: 1 – single-pole model of an ideal converter; 2 – single-pole model of a non-ideal converter; 3 – two-pole model of an ideal converter; 4 – proposed two-pole model of a non-ideal converter; \circ – simulation results; \bullet – measurement results

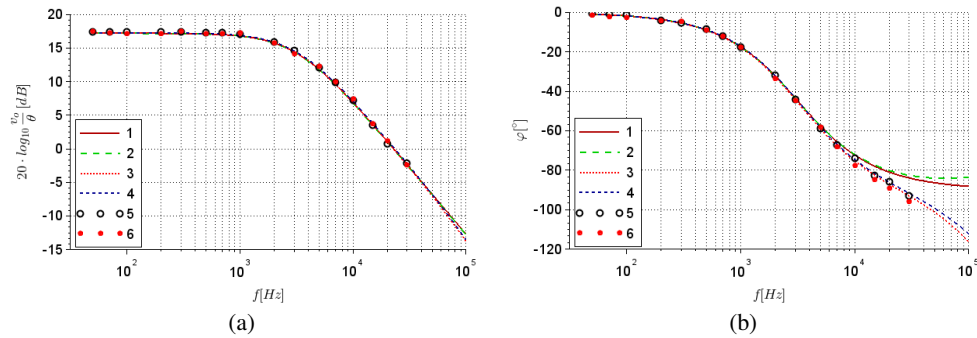


Fig. 14. Control-to-output (H_d) frequency characteristics of the buck buck_1 converter working in DCM with duty cycle $D_A = 0.4$. The curves correspond to: 1 – single-pole model of an ideal converter; 2 – single-pole model of a non-ideal converter; 3 – two-pole model of an ideal converter; 4 – proposed two-pole model of a non-ideal converter; \circ – simulation results; \bullet – measurement results

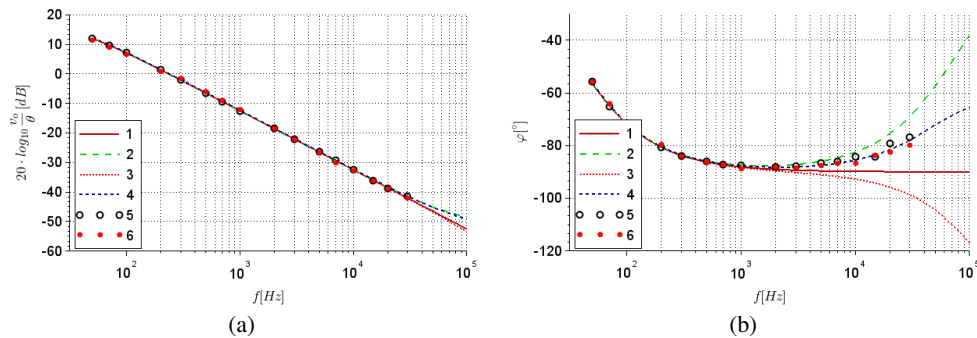


Fig. 15. Control-to-output (H_d) frequency characteristics of the buck_2 converter working in DCM with duty cycle $D_A = 0.4$. The curves correspond to: 1 – single-pole model of an ideal converter; 2 – single-pole model of a non-ideal converter; 3 – two-pole model of an ideal converter; 4 – proposed two-pole model of a non-ideal converter; \circ – simulation results; \bullet – measurement results

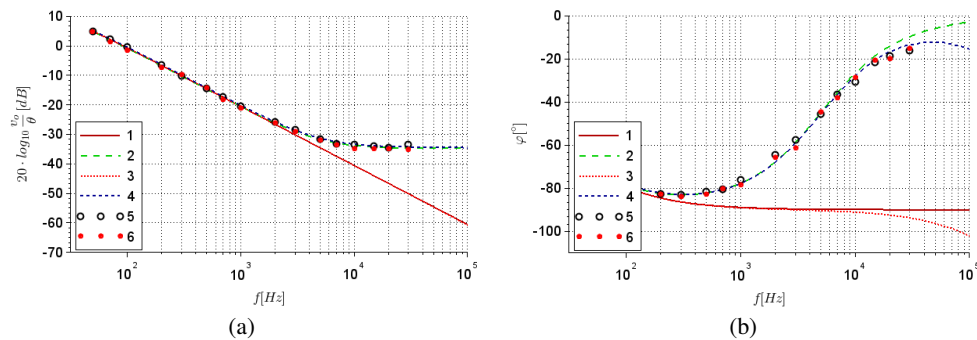


Fig. 16. Control-to-output (H_d) frequency characteristics of the buck_3 converter working in DCM with duty cycle $D_A = 0.4$. The curves correspond to: 1 – single-pole model of an ideal converter; 2 – single-pole model of a non-ideal converter; 3 – two-pole model of an ideal converter; 4 – proposed two-pole model of a non-ideal converter; \circ – simulation results; \bullet – measurement results

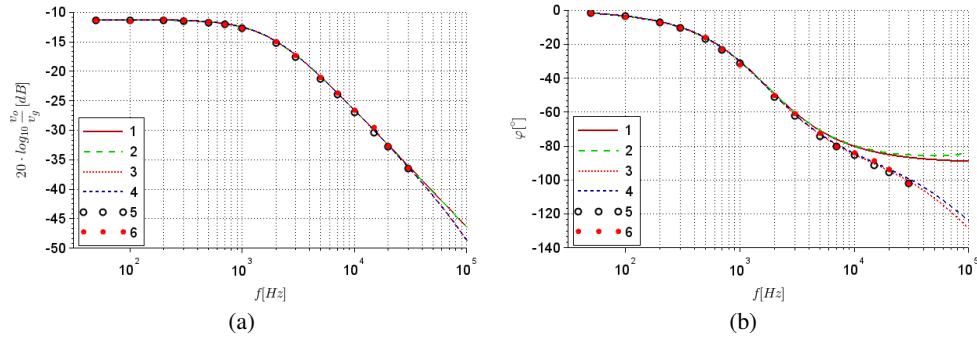


Fig. 17. Input-to-output (H_g) frequency characteristics of the buck_1 converter working in DCM with duty cycle $D_A = 0.1$. The curves correspond to: 1 – single-pole model of an ideal converter; 2 – single-pole model of a non-ideal converter; 3 – two-pole model of an ideal converter; 4 – proposed two-pole model of a non-ideal converter; \circ – simulation results; \bullet – measurement results

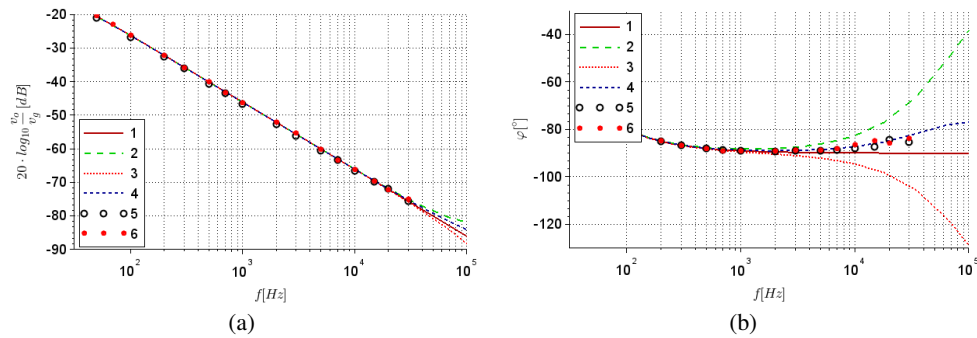


Fig. 18. Input-to-output (H_g) frequency characteristics of the buck_2 converter working in DCM with duty cycle $D_A = 0.1$. The curves correspond to: 1 – single-pole model of an ideal converter; 2 – single-pole model of a non-ideal converter; 3 – two-pole model of an ideal converter; 4 – proposed two-pole model of a non-ideal converter; \circ – simulation results; \bullet – measurement results

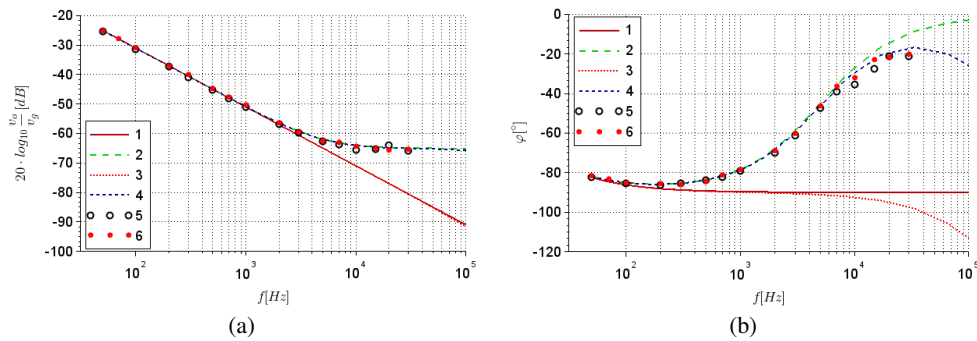


Fig. 19. Input-to-output (H_g) frequency characteristics of the buck_3 converter working in DCM with duty cycle $D_A = 0.1$. The curves correspond to: 1 – single-pole model of an ideal converter; 2 – single-pole model of a non-ideal converter; 3 – two-pole model of an ideal converter; 4 – proposed two-pole model of a non-ideal converter; \circ – simulation results; \bullet – measurement results

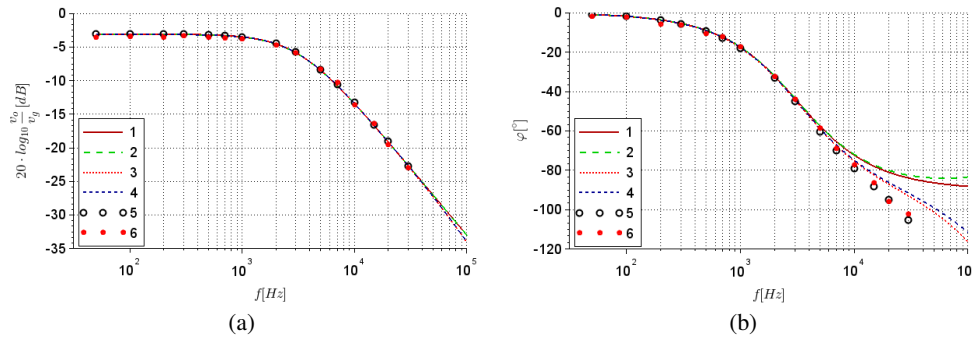


Fig. 20. Input-to-output (H_g) frequency characteristics of the buck_1 converter working in DCM with duty cycle $D_A = 0.4$. The curves correspond to 1 – single-pole model of an ideal converter; 2 – single-pole model of a non-ideal converter; 3 – two-pole model of an ideal converter; 4 – proposed two-pole model of a non-ideal converter; \circ – simulation results; \bullet – measurement results

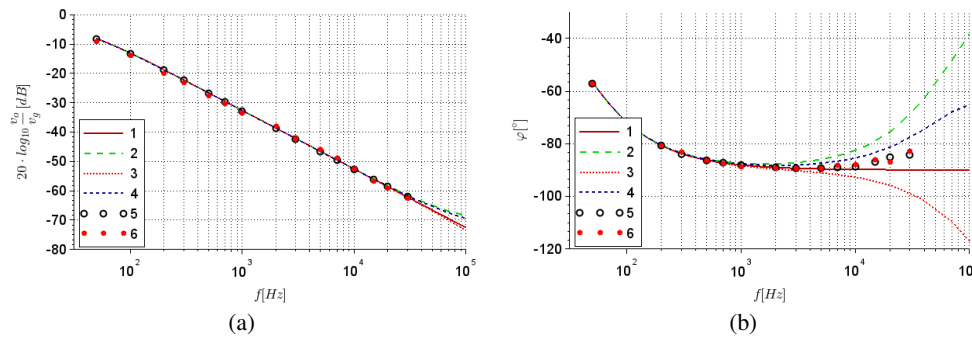


Fig. 21. Input-to-output (H_g) frequency characteristics of the buck_2 converter working in DCM with duty cycle $D_A = 0.4$. The curves correspond to 1 – single-pole model of an ideal converter; 2 – single-pole model of a non-ideal converter; 3 – two-pole model of an ideal converter; 4 – proposed two-pole model of a non-ideal converter; \circ – simulation results; \bullet – measurement results

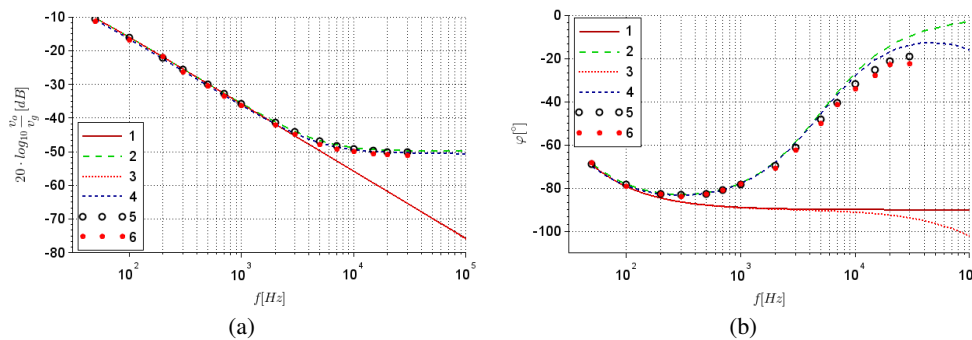


Fig. 22. Input-to-output (H_g) frequency characteristics of the buck_3 converter working in DCM with duty cycle $D_A = 0.4$. The curves correspond to 1 – single-pole model of an ideal converter; 2 – single-pole model of a non-ideal converter; 3 – two-pole model of an ideal converter; 4 – proposed two-pole model of a non-ideal converter; \circ – simulation results; \bullet – measurement results

4.2. Discussion

The results of the calculations show large discrepancies between the models. However, most of the models, except for the single-pole model of an ideal converter, showed good consistency with some of the simulation and measurement results.

Such consistency can be observed with the single-pole models of a non-ideal converter (curve 2) and the simulation results shown in Figs. 13, 16, 19 and 22. The figures refer to the buck_3 converter which was designed in a way to move the second pole to much higher frequencies than the switching frequency, therefore making its influence on the frequency characteristics negligible. The zero of the transfer function, on the other hand, was set at relatively low frequencies which has a strong impact on the characteristics. In this case, the single-pole model of a non-ideal converter seems to be more accurate than the two-pole model of an ideal converter. However, when the pole is moved closer to the switching frequency, its influence on the frequency characteristics becomes noticeable as in the buck_2 example shown in Figs. 12, 15, 18 and 21. In this case, neither of the two models can predict the frequency characteristics. Better accuracy in this case can be observed with the single-pole model of an ideal converter (curve 1). Finally, when the second pole is moved to relatively low frequencies and the zero is set at high frequencies, as in the buck_1 converter, the two-pole transfer functions of an ideal converter start to show good consistency with the simulation and measurement results (Figs. 11, 14, 17 and 20).

The single-pole model of an ideal converter didn't predict the behaviour of any of the simulated converters however, if the components were chosen differently this model could also be validated. On the other hand, the proposed control-to-output and input-to-output transfer functions (curves 4 in Figs. 11–22) show good consistency with all of the simulations and measurement results.

It can be observed that based on the element values used in the converters (the position of the poles and zeros) it is possible to design a converter that could be described with a single-pole model that includes non-ideal elements (Figs. 19 and 22), or a two-pole model of an ideal converter (Figs. 17 and 20). The single pole model of an ideal converter is not accurate with any of the measured converters since it doesn't include the second pole, nor the zero related to the ESR of the output capacitor. However, if different component values were chosen, it would be possible to design a converter that could be described with the model. Nevertheless, it can be noticed that the measured characteristics show good consistency with the proposed model for all of the measured converters, even for specially designed case presented in Figs. 12, 15, 18 and 21. Therefore it can be stated that the proposed models can predict the behaviour of the simulated converters, regardless of the relation between the poles and zeros of the transfer function. Some discrepancies can be observed between the model and the simulation and measurement results. The differences can be related to the limited resolution of the oscilloscope (especially at high frequencies where the signal-to-noise ratio is small), and the accuracy of the model. The model is an approximation of the real system, and even though it takes into account the nonlinearities of the system (by performing the linearization step) it still can be affected by the nonlinearities related to the semiconductor elements.

5. Conclusions

This paper presents small-signal models of a non-ideal buck converter, working in discontinuous conduction mode. The presented formulas include the input-to-output and control-to-output transfer functions, which are compared with the frequency characteristics acquired through OrCAD

simulations and by measurements. The results presented in this paper show that existing models in form of transfer functions can predict the behaviour of a buck converter for specific conditions only. The specific conditions are related to the position of the poles and zeros in the transfer functions. The location of the second pole can be calculated using well-known two-pole model of an ideal converter. However, the zero exists in the transfer function only when ESR value of the output capacitor is taken into consideration. The simulations and measurements show that the location of zero has a significant impact on the frequency characteristics. By moving the poles and zeros it is possible to design a converter that can be described using transfer functions that exist in the literature. However, the results presented in this paper show that none of the existing models can predict the frequency characteristics of the second converter used in the simulation (buck_2), except for the proposed models. It was presented that the proposed models feature good consistency with all of the simulation results, regardless of the converter parameters. The impact of the other parasitic resistances on the frequency characteristics was not measured and is left for future evaluation.

A. Appendix A

This section includes the list of symbols used in the paper (Table A1) as well as the coefficients of the proposed transfer functions.

Table A1. List of the used symbols

Symbol	Description
d_A	Large-signal value of the duty cycle
D_A	Quiescent value of the duty cycle
d_a	Small-signal value of the duty cycle
$\theta(s)$	Small-signal value of the duty cycle in 's' domain
t_{ON}	Time interval when the transistor switch is ON
T_S	Period of the PWM signal
f_S	Switching frequency of the PWM signal
i_{LAV}	Average value of the inductor current, calculated for a single period
$i_{LAV(ON)}$	Average value of the inductor current, calculated for the ON phase
$i_{LAV(OFF1)}$	Average value of the inductor current, calculated for the OFF1 phase
i_{Lpk}	Peak value of the inductor current
$I_l(s)$	Small-signal value of the inductor current in 's' domain
R_L	Equivalent series resistance of the inductor
R_T	Equivalent series resistance of the transistor switch
R_C	Equivalent series resistance of the output capacitor
R_D	Equivalent series resistance of the diode

Continued on next page

Table A1 – *Continued from previous page*

Symbol	Description
R_{LOAD}	Resistance value of the load resistor
v_{IN}	Large-signal value of the input voltage
V_{IN}	Quiescent value of the input voltage
v_{in}	Small-signal value of the input voltage
$V_{in}(s)$	Small-signal value of the input voltage in 's' domain
v_{OUT}	Large-signal value of the output voltage
v_{OUT}	Quiescent value of the output voltage
v_{out}	Small-signal value of the output voltage
$v_{OUT}(s)$	Small-signal value of the output voltage in 's' domain
M_V	The ratio between the output and input voltage
M_I	The ratio between the input and output voltage
φ	Phase shift between the sinusoidal signal v_{SIN} and output voltage
$H_d(s)$	Control-to-output transfer function
$H_g(s)$	Input-to-output transfer function

All of the coefficients that exist in (23) and (24) can be calculated using Formulas (A.1)–(A.11)

$$G = \frac{1}{R_{LOAD}}, \tag{A.1}$$

$$C_Z = C(1 + GR_C), \tag{A.2}$$

$$R_G = \frac{2L}{T_S}, \tag{A.3}$$

$$G_Z = \frac{1}{R_G} = \frac{T_S}{2L}, \tag{A.4}$$

$$R_P = R_T + R_L = R_D + R_L, \tag{A.5}$$

$$R_{PG} = D_A R_P + R_G, \tag{A.6}$$

$$G_A = D_A^2 G_Z, \tag{A.7}$$

$$M_V = \frac{V_{OUT}}{V_{IN}} = \frac{2}{(R_P G + 1) \left(1 + \sqrt{1 + 4 \frac{G}{G_A (R_P G + 1)}} \right)}, \tag{A.8}$$

$$M_I = \frac{1}{M_V}, \tag{A.9}$$

$$K = M_I - 1, \tag{A.10}$$

$$R_Y = R_G \frac{M_V}{D_A} + R_P. \tag{A.11}$$

References

- [1] Kalson S., Kar S.R., *Comparison of Buck Converter Control Methods*, 2022 2nd International Conference on Intelligent Technologies (CONIT), Hubli, India, pp. 1–8 (2022), DOI: [10.1109/CONIT55038.2022.9847851](https://doi.org/10.1109/CONIT55038.2022.9847851).
- [2] Marey A., Bhaskar M.S., Almahles D., Mostafa H., *Analytical Solution for Transient Reactive Elements for DC–DC Converter Circuits*, *Electronics*, vol. 11, no. 19, 3121, pp. 1–19 (2022), DOI: [10.3390/electronics11193121](https://doi.org/10.3390/electronics11193121).
- [3] Khan M.U., Murtaza A.F., Noman A.M., Sher H.A., Zafar M., *State-Space Modeling, Design, and Analysis of the DC–DC Converters for PV Application: A Review*, *Sustainability*, vol. 16, no. 1, 202 pp. 1–20 (2024), DOI: [10.3390/su16010202](https://doi.org/10.3390/su16010202).
- [4] Middlebrook R.D., Cuk S., *A General Unified Approach to Modelling Switching-Converter Power Stages*, *IEEE Power Electronics Specialists Conference Cleveland, OH*, pp. 73–86 (1976), DOI: [10.1109/PESC.1976.7072895](https://doi.org/10.1109/PESC.1976.7072895).
- [5] Sun J., Mitchell D.M., Greuel M.F., Krein P.T., Bass R.M., *Averaged Modelling of PWM Converters Operating in Discontinuous Conduction Mode*, *IEEE Transactions on Power Electronics*, vol. 16, no. 4, pp. 482–492 (2001), DOI: [10.1109/63.931052](https://doi.org/10.1109/63.931052).
- [6] Davoudi A., Jatskevich J., Rybel T.S., *Numerical state-space average-value modelling of PWM DC–DC converters operating in DCM and CCM*, *IEEE Trans. Power Electron.*, vol. 21, no. 4, pp. 1003–1012 (2006), DOI: [10.1109/TPEL.2006.876848](https://doi.org/10.1109/TPEL.2006.876848).
- [7] Usman Iftikhar M., Lefranc P., Sadarnac D., Karimi C., *Theoretical and Experimental Investigation of Averaged Modelling of Non-ideal PWM DC–DC Converters Operating in DCM*, *IEEE Power Electronics Specialists Conference (PESC)*, pp. 2257–2263 (2008), DOI: [10.1109/PESC.2008.4592277](https://doi.org/10.1109/PESC.2008.4592277).
- [8] Vorperian V., *Simplified Analysis of PWM Converters using Model of PWM Switch Part I: Continuous Conduction Mode*, *IEEE Transactions on Aerospace and Electronic Systems*, vol. 26, no. 3, pp. 490–496 (1990), DOI: [10.1109/7.106126](https://doi.org/10.1109/7.106126).
- [9] Vorperian V., *Simplified analysis of PWM converters using the model of the PWM switch Part II: Discontinuous Conduction Mode*, *IEEE Transactions on Aerospace and Electronic Systems*, vol. 26, no. 3, pp. 497–505 (1990), DOI: [10.1109/7.106127](https://doi.org/10.1109/7.106127).
- [10] Czarkowski D., Kazimierczuk M.K., *Energy-conservation approach to modelling PWM DC–DC converters*, *IEEE Transactions on Aerospace and Electronic Systems*, vol. 29, no. 3, pp. 1059–1063 (1993), DOI: [10.1109/7.220955](https://doi.org/10.1109/7.220955).
- [11] Janke W., *Averaged models of pulse-modulated DC–DC power converters. Part II. Models based on the separation of variables*, *Archives of Electrical Engineering*, vol. 61, no. 4, pp. 633–654 (2012), DOI: [10.2478/v10171-012-0046-7](https://doi.org/10.2478/v10171-012-0046-7).
- [12] Davoudi A., Jatskevich J., *Realization of Parasitics in State-Space Average-Value Modelling of PWM DC–DC Converters*, *IEEE Transactions on Power Electronics*, vol. 21, no. 4, pp. 1142–1147 (2006), DOI: [10.1109/TPEL.2006.879048](https://doi.org/10.1109/TPEL.2006.879048).
- [13] Biolkova V., Kolka Z., Biolk D., *State-Space Averaging (SSA) Revisited: On the Accuracy of SSA-Based Line-To-Output Frequency Responses of Switched DC–DC Converters*, *WSEAS Transactions on Circuits and Systems*, vol. 9, no. 2, pp. 81–90 (2010).
- [14] Jha V., Rai P., *State Space Averaged Modelling of Basic Converter Topologies*, *VSRD International Journal of Electrical, Electronics & Communication Engineering*, vol. 2, no. 8, pp. 566–575 (2012).
- [15] Priewasser R., Unterrieber C., Marsili S., Huemer M., *Modelling, Control, and Implementation of DC–DC Converters for Variable Frequency Operation*, *IEEE Transactions on Power Electronics*, vol. 29, no. 1, pp. 287–301 (2014), DOI: [10.1109/TPEL.2013.2248751](https://doi.org/10.1109/TPEL.2013.2248751).

- [16] Hassan M.S., Elbaset A.A., *Small-Signal MATLAB/Simulink Model of DC–DC Buck Converter using State-Space Averaging Method*, 17th International Middle East Power Systems Conference, Mansoura University, Egypt, pp. 1–8 (2015), DOI: [10.1007/978-3-319-47464-9_5](https://doi.org/10.1007/978-3-319-47464-9_5).
- [17] Modabbernia M.R., *The State Space Average Model of Buck-Boost Switching Regulator Including all of The System Uncertainties*, International Journal on Computer Science and Engineering (IJCSE), vol. 5, no. 2, pp. 120–132 (2013).
- [18] Abdelgawad H., Sood V., *Average Model of Boost Converter, including Parasitics, operating in Discontinuous Conduction Mode (DCM)*, International Journal on Power Engineering and Energy (IJPEE), vol. 7, no. 2, pp. 636–646 (2016).
- [19] Mishra S.K., *Design-oriented analysis of modern active droop-controlled power supplies*, IEEE Transactions on Industrial Electronics, vol. 56, no. 9, pp. 3704–3708 (2009), DOI: [10.1109/TIE.2009.2025289](https://doi.org/10.1109/TIE.2009.2025289).
- [20] González I., Sánchez-Squella A., Langarica-Cordoba D., Yanine-Misleh F., Ramirez V., *A PI + Sliding-Mode Controller Based on the Discontinuous Conduction Mode for an Unidirectional Buck–Boost Converter with Electric Vehicle Applications*, Energies, vol. 14, 6785 (2021), DOI: [10.3390/en14206785](https://doi.org/10.3390/en14206785).
- [21] Janke W., *Impulsowe przetwornice napięcia stałego*, ISBN 978-83-7365-341-2, Wydawnictwo Uczelniane Politechniki Koszalińskiej (in Polish), Koszalin (2014).
- [22] Middlebrook R.D., Cuk S., *A General Unified Approach to Modelling Switching-Converter Power Stages*, IEEE Power Electronics Specialists Conference Cleveland, OH, pp. 73–86 (1976), DOI: [10.1109/PESC.1976.7072895](https://doi.org/10.1109/PESC.1976.7072895).
- [23] Rim C.T., Joung G.B., Cho G.H., *Practical Switch Based State-Space Modelling of DC–DC Converters with All Parasitics*, IEEE Transactions on Power Electronics, vol. 6, no. 4, pp. 611–617 (1991), DOI: [10.1109/63.97759](https://doi.org/10.1109/63.97759).
- [24] Walczak M., *Modelowanie i badania wybranych impulsowych przetwornic napięcia stałego, pracujących w trybie nieciągłego przewodzenia (DCM)*, Phd Thesis (in Polish), Department of Electronics and Computer Science, Technical University of Technology in Koszalin, Koszalin (2019).
- [25] Erickson R.W., Maksimović D., *Fundamentals of power electronics*, Second Edition, ISBN 0-7923-7270-0, sixth printing (2004).
- [26] Mehta V., Malik P., *Comparison between Asynchronous and Synchronous Buck Converter Topology*, International Journal of Applied Engineering Research, vol. 7, no. 11, pp. 1–4 (2012).
- [27] Janke W., Walczak M., *Influence of output conductance on characteristic frequencies of switch mode BUCK and BOOST converter*, Archives of Electrical Engineering, vol. 66, no. 1, pp. 165–178 (2017), DOI: [10.1515/ae-2017-0012](https://doi.org/10.1515/ae-2017-0012).
- [28] Walczak M., *Methods of DC/DC converter transfer function measurements, based on data acquired in the time domain*, Metrology and Measurement Systems, vol. 4, pp. 661–671 (2019), DOI: [10.24425/mms.2019.130569](https://doi.org/10.24425/mms.2019.130569).